

## Ultrasonic spray deposition for production of organic solar cells

K. Xerxes Steirer<sup>a,b,\*</sup>, Matthew O. Reese<sup>b</sup>, Benjamin L. Rupert<sup>b</sup>, Nikos Kopidakis<sup>b</sup>, Dana C. Olson<sup>b</sup>, Reuben T. Collins<sup>a</sup>, David S. Ginley<sup>b</sup>

<sup>a</sup> Colorado School of Mines, 1500 Illinois Street, Golden, CO 80401, USA

<sup>b</sup> National Renewable Energy Laboratory, 1617 Cole Boulevard, Golden, CO 80401, USA

### ARTICLE INFO

#### Article history:

Received 12 September 2008

Received in revised form

29 October 2008

Accepted 30 October 2008

Available online 24 December 2008

#### Keywords:

Bulk heterojunction

Organic

Photovoltaic

Spray

Deposition

Process

### ABSTRACT

Recent improvements of organic photovoltaic power conversion efficiencies have motivated development of scalable processing techniques. We compare chlorobenzene and *p*-xylene, as solvents with similar bulk properties, in a case study of ultrasonic spray depositions of bulk heterojunction layers in photovoltaic devices. Structure and morphology of spray-deposited films are investigated via small-angle X-ray diffraction and optical microscopy. Unique phases are observed in bulk heterostructure films sprayed from *p*-xylene. Films sprayed from chlorobenzene resulted in higher device efficiencies than *p*-xylene due to large differences in film morphologies. Carrier loss mechanisms are also investigated. Post-production annealing increases power conversion efficiency to 3.2% when chlorobenzene is used.

© 2008 Published by Elsevier B.V.

### 1. Introduction

Organic photovoltaics produced by roll-to-roll manufacturing methods may allow for an ultra-low cost solar energy conversion technology. Since the discoveries of photoactive polymers [1], ultrafast charge transfer from polymer to fullerene [2] and the bulk heterojunction concept [3,4] a concerted effort has been put forth to increase the efficiency of these devices. Current certified efficiencies of organic photovoltaic (OPV) devices are up to 5.15% for large 1 cm<sup>2</sup> device area [5] and 5.9% for small device areas [6] while reports of stability and lifetimes are gaining attention [7,8]. The workhorse OPV approach in recent years has used blends of polymers and fullerenes to create a bulk heterojunction absorber layer. In this approach, well defined, interspersed polymer-rich and fullerene-rich domains act as dual pathways for conduction of oppositely charged carriers to their respective electrodes. The relative domain size, purity and structure affect many of the device properties and ultimately power conversion efficiency (PCE). The benefits of an organic absorber layer are low manufacturing costs from flexible solution processing and potential increase in efficiency due to synthetically tunable electronic and optical properties. However, spin coating methods conventionally used to deposit laboratory-scale OPV devices are

generally not scalable. Given the rapid advance of OPV conversion efficiencies attention has been directed toward the development of large area device fabrication techniques [9–11].

Historically, spray deposition has been used in the coating industry for a myriad of applications typically achieving uniform films at low cost including multilayer paints for automobiles, plastic coating and even some electronic materials such as lead zirconate titanate and barium strontium titanate. Spray technologies have recently been shown as compatible with functional organic thin film depositions. A PCE of 2.83% has been reported for a spray-deposited OPV device [10]. These devices were made by an inexpensive handheld airbrush technique used to deposit the active layer.

In this paper we discuss the development of ultrasonic spray deposition of bulk heterojunction OPVs. Ultrasonic spray deposition is a relatively new variant of conventional spray approaches but has many strengths including picoliter drop sizes, directional spray deflection with an inert gas, large area uniform coverage for very thin films and the potential for simultaneous multi-component deposition from ganged heads. The ultrasonic spray deposition system used in this study is shown schematically in Fig. 1a. An ultrasonicated surface incorporated into the spray nozzle is used in conjunction with a tri-phase solution flow pump and an inert carrier gas to deposit solution onto the substrate. Computer control allows reproducible depositions with precise deposition rates. Optimization of film thickness is quickly done through layer-by-layer spray deposition. The individual droplets produced by the ultrasonic nozzle are similar in size to those

\* Corresponding author at: National Renewable Energy Laboratory, 1617 Cole Boulevard, Golden, CO 80401, USA. Tel.: +1 303 384 6484; fax: +1 303 384 6430.

E-mail address: [ken\\_steirer@nrel.gov](mailto:ken_steirer@nrel.gov) (K.X. Steirer).

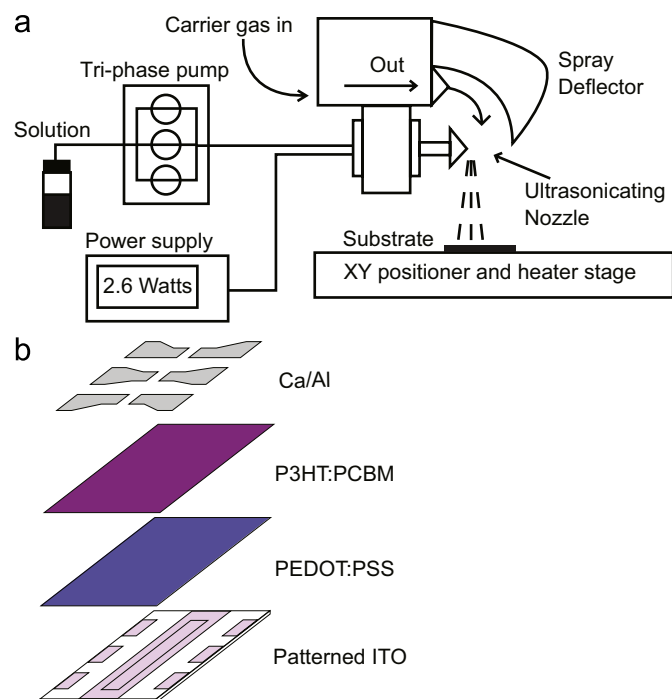


**Fig. 1.** (a) Ultrasonic sprayer schematic showing carrier gas directing ultrasonically formed droplets onto the substrate. (b) Device architecture for OPV devices with active layers ultrasonically sprayed using chlorobenzene or *p*-xylene as the solvent. Sandwich structure is ITO/PEDOT:PSS/P3HT:PCBM/Ca/Al.

produced using an inkjet nozzle. The nozzle is designed to operate clog-free over a wide range of solution concentrations from the dilute to concentrated.

This system was used to deposit the bulk heterojunction active layer in a series of OPV devices. Fabrication began with a conventional OPV process using an indium tin oxide (ITO)-coated glass substrate which was spin coated with a hole blocking poly(3,4-ethylenedioxythiophene):polystyrene sulfonate (PEDOT:PSS) layer. The spray-deposited active layer which followed was comprised of a blend of poly(3-hexylthiophene) (P3HT) and [6,6] phenyl C<sub>61</sub> butyric methyl ester (PCBM). A Ca/Al back contact was then thermally deposited. The device architecture is depicted in Fig. 1b. This device design when an optimized active layer is deposited by spin coating, has regularly been reported to achieve certified efficiencies near 4% [12,13]. In the present study we compare active layer films ultrasonically sprayed from chlorobenzene and *p*-xylene as solvents. Previous reports on P3HT:PCBM solutions utilizing *p*-xylene as a solvent have shown the formation of nanofibrillar aggregates due to the relative nonpolar nature of the solvent. Multiple processing steps have yielded high-efficiency devices made with *p*-xylene [14,15]. BHJ films spin coated from chlorobenzene have also resulted in favorable morphology when additives or post-processing is utilized [16]. These solvents have largely different dipole moments but, similar boiling points, vapor pressures and surface tensions, which makes them a good case study for spray depositions. It has been shown that boiling point and vapor pressure of the solvent affect the structure and phase segregation properties of BHJ films [11,13,17,18]. We show here that the solvent–solute interaction plays an important role when the BHJ solution is sprayed. We have structurally examined BHJ films ultrasonically sprayed from chlorobenzene and *p*-xylene and have found unique phases in the *p*-xylene system. Absorption spectra for each system show enhanced polymer ordering and aggregation combined with significant absorption loss of high energy photons for the *p*-xylene system, presumably due to the

formation of very large PCBM grains that may not fully interconnect with the polymer phase. We have fabricated devices from each system and show greater performance from the films sprayed from chlorobenzene. We analyze loss mechanisms via illumination intensity-dependent short circuit current and large reverse bias current measurements for each system. Finally, we demonstrate a PCE of 3.2% when device active layers are sprayed from chlorobenzene and a flood layer is imposed to reduce surface roughness.

## 2. Experiment

### 2.1. Materials

Baytron P VP Al 4083, PEDOT:PSS was obtained from HC Starck and was filtered through a 0.45 μm filter prior to use. P3HT was obtained from Rieke and PCBM from Nano-C. Active layer materials were stored in an inert atmosphere and used as received. Anhydrous *p*-xylene and chlorobenzene from Aldrich were purged with nitrogen to remove any residual oxygen and stored in an inert atmosphere prior to use.

### 2.2. Device fabrication

OPV devices were fabricated with pre-patterned ITO on glass substrates (Colorado Concept Coatings) to define the bottom electrodes. Patterned substrates were scrubbed with an ultrasonic brush using a liquinox/DI water solution and then rinsed in DI water. Following the DI water rinse, they were further cleaned in ultrasonic baths of acetone and then isopropanol. Finally, an oxygen plasma surface treatment of 155 W for 5 min was applied. Thin films of PEDOT:PSS were spin coated onto the prepared ITO substrates at 4000 rpm. PEDOT:PSS-coated substrates were heated at 120 °C for 1 h in air. The BHJ solution was prepared in a nitrogen atmosphere and utilized a 1:1 ratio of P3HT:PCBM diluted to 2 mg/mL in chlorobenzene or *p*-xylene. Solutions were stirred on a hotplate held at 60 °C for several hours. After mixing, the solutions were allowed to cool and set for >24 h. The active layer was then ultrasonically spray deposited in a nitrogen glove box with the concentration of H<sub>2</sub>O < 0.1 ppm and of O<sub>2</sub> ~5.0 ppm. For deposition of the ultrasonically spray-coated BHJ films we used a Sonotek ultrasonic spray nozzle #8700-120, Omega Engineering mass flow regulator and a Fluid Metering Inc. VMP Tri reversible flow pump. Active layers were composed of 50 layers, each sprayed at 0.33 mL/min having a carrier gas flow of 7 L/min. The nozzle was 5 cm from the substrate held at 25 °C. Individual layers sprayed from the chlorobenzene solution had average thicknesses of 11 ± 1 nm. Two additional flood layers where the solution flow rate was doubled were added to some chlorobenzene-sprayed films to investigate the smoothing effect. Some *p*-xylene-sprayed films were deposited at 78 °C to eliminate large crystallite formations in these films. The optimized parameters were chosen solely dependent upon measured PCE values of chlorobenzene-deposited devices. Electrodes of Ca/Al (20 nm/100 nm) were then thermally evaporated through shadow masks in an integrated dry box system resulting in 0.11 cm<sup>2</sup> device areas. Post-production annealing was performed on a digitally controlled hotplate at 110 °C for 10 min.

### 2.3. Measurement

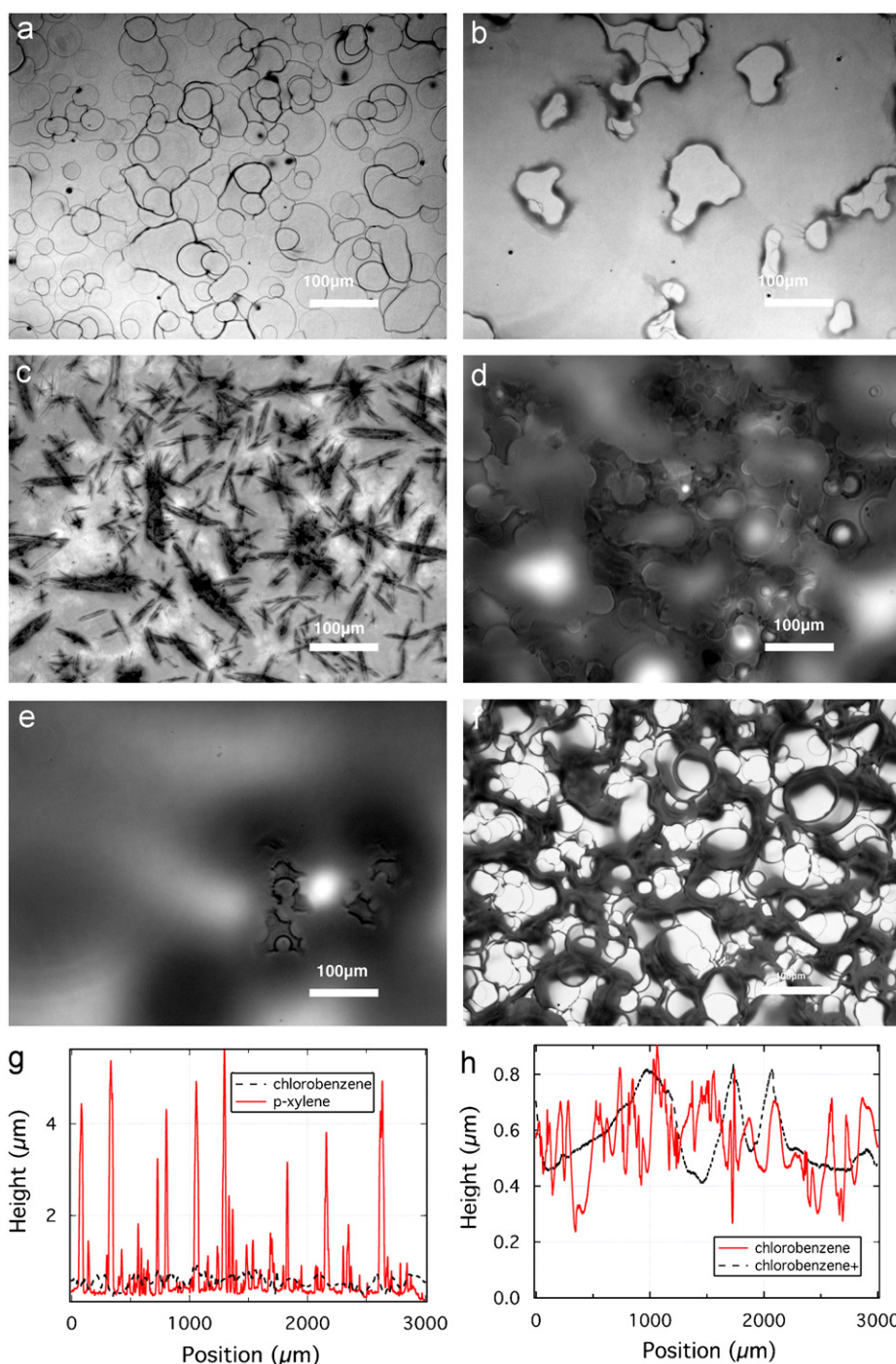
X-ray diffraction (XRD) measurements were performed with a Scintag PTS goniometer (Bragg–Brentano geometry) using Cu Kα radiation of wavelength 0.154 nm detected with a liquid nitrogen

**Table 1**Bulk solvent properties for chlorobenzene and *p*-xylene.

Solvent	Boiling point (°C)	Vapor pressure (mmHg)	Surface tension (dynes/cm)	Dipole moment (D)
Chlorobenzene	132	11.8	33.6	1.69
<i>p</i> -Xylene	138	9	28.4	0.07

[a,b], 1 dyne =  $10^{-5}$  N, 1 mm Hg = 133.3 Pa, 1 D =  $3.3356 \times 10^{-30}$  C m.

a: R.C. Weast and M.J. Astle, W.H. Beyer (Eds.), CRC Handbook of Physics and Chemistry, 69th ed, CRC Press, Boca Raton, FL, 1988.

b: Sigma Aldrich, Product Catalog, Accessed on [www.sigmaaldrich.com](http://www.sigmaaldrich.com), 25 August 2008.

**Fig. 2.** (a) Dark field microscope image of a single-layer-sprayed BHJ from chlorobenzene. Dark rings represent BHJ material. Light area represents the base substrate layer. (b) Dark field microscope image of a single-layer-sprayed BHJ from *p*-xylene. The light area represents the base substrate while the dark and shadowed region is BHJ. (c) Dark field microscope image of 50 layers sprayed BHJ from *p*-xylene. Dark crystalline structures are evident and exhibit a higher optical density than the surrounding film. (d) Dark field microscope image of 50 layers sprayed BHJ from chlorobenzene. Lighter areas represent thinner film regions. Although some drop uniting is shown, coffee stain effects are prominent. (e) Dark field microscope image of 50 layers plus flood layers sprayed BHJ from chlorobenzene. (f) Dark field microscope image of 50 layers sprayed BHJ from *p*-xylene with the substrate held at 78 °C. (g) Line profiles of chlorobenzene and *p*-xylene-sprayed BHJ films taken with stylus profilometry. Large crystallites are formed in *p*-xylene films. (h) Line profiles of BHJ films sprayed from chlorobenzene with and without the two flood layers having measured average thicknesses of 0.55 and 0.58  $\mu\text{m}$ , respectively. A higher deposition rate at the end of the deposition sequence results in a smoother texture.



cooled germanium detector. The scan rate was  $0.8^\circ/\text{min}$  from  $3^\circ$  to  $40^\circ$  in  $2\theta$  in  $0.025^\circ$  steps. Thick ( $2\text{--}4\ \mu\text{m}$ ) BHJ films were deposited onto  $1'' \times 1''$  quartz substrates (Gem Dugout) cut  $6^\circ$  from (0001) that gave a low-background signal in the XRD measurement. Film thicknesses were measured with a Dektak 8 stylus profilometer and used to normalize the diffraction spectra.

Device testing was performed in an inert atmosphere in dark or one Sun conditions. Light intensity was monitored with a filtered silicon photodiode (Hamamatsu S1787-04) calibrated by NREL's Measurement and Characterization group. Short circuit current densities were confirmed on a second solar simulator and were also consistent, to within a few percent, with integrated incident photon-to-current efficiency (IPCE) spectra. IPCE measurements were performed in an inert environment by illuminating samples with light from a 300 W Xe lamp filtered by a monochromator. Light intensities below one Sun were achieved with metallic reflective neutral density filters (Melles Griot). Voltage-dependent current measurements were taken with a Keithley 236 source measurement unit.

### 3. Results and discussion

The role of solvents on film formation has been linked to boiling point, vapor pressure, polarity and surface tension [11,17,18]. Here we have chosen two solvents, chlorobenzene and *p*-xylene for direct comparison. Table 1 summarizes the characteristics of these solvents illustrating small differences in boiling point, vapor pressure, surface tension and a large difference in dipole moment.

We have observed notable differences in wetting and film formation from each solvent. Fig. 2a shows the morphology improvements due to increased wetting of a single deposited layer from *p*-xylene while Fig. 2b shows the dominant coffee-stained texture [19] of the chlorobenzene-deposited layer. The lower surface tension of the *p*-xylene solution enhances wetting and, hence, uniting of drops on the substrate. This aids in the formation of more uniform coverage. However, as additional layers are sprayed, building up a multilayer film as is typical in spray depositions [10,11,20], crystal aggregates begin to nucleate out of the film as displayed in Fig. 2c disrupting the smooth film morphology usually seen in spin-coated BHJ films. The chlorobenzene-sprayed multilayer film is shown in Fig. 2d. This film was  $0.55\ \mu\text{m}$  thick, shows some evidence of drops coalescing and in general, exhibits morphology similar to its single-layer film whereas the *p*-xylene-sprayed multilayer film does not. Profiles of films sprayed from *p*-xylene and chlorobenzene are compared in Fig. 2e and show the increased film texturing due to the crystal formations. Doubling the deposition rate of the chlorobenzene solution and adding two additional flood layers at the end of the sequence effectively smoothes the chlorobenzene-sprayed film as shown in Fig. 2e and resulted in a film thickness of  $0.58\ \mu\text{m}$ . Profiles for the chlorobenzene-sprayed films are compared in Fig. 2h and show the smoothing effect of the additional flood layers. Increasing the *p*-xylene solution deposition rate for the final layers did not reduce texturing for *p*-xylene films. However, increased substrate temperature stopped crystal formation in films sprayed from the *p*-xylene solution but also resulted in predominant coffee stain effects shown in Fig. 2f. These four films from different depositions, two from chlorobenzene, one with flooding and two from *p*-xylene, one deposited at higher temperature are the focus of our study here.

UV-vis absorption spectra were taken for well-mixed solutions of P3HT:PCBM in either *p*-xylene or chlorobenzene after standing at room temperature ( $22^\circ\text{C}$ ) in a nitrogen glove box for 5 and 96 h. The spectra shown in Fig. 3a are normalized so that the isotropic

PCBM absorption peak at 325 nm has the same magnitude in each spectrum [21]. The *p*-xylene solution shows enhanced relative absorption around 615 nm, indicative of increased order and aggregation of the polymer phase and delocalization of excitonic states [22,23] while the chlorobenzene solution shows no enhanced absorption. Absorption spectra for sprayed films from both solvents deposited at  $25^\circ\text{C}$  in Fig. 3b show evidence of significantly enhanced polymer ordering coupled with a large decrease of shorter wavelength photon absorption in the *p*-xylene-sprayed films. The crystal structures have higher optical densities than the surrounding film as is evidenced in Fig. 2c. Thus a large fraction of the material is located in the crystallites and results in absorption loss. These spectra along with aforementioned studies indicate that aggregates are nucleated and preformed in the *p*-xylene solution and grow as multiple layers are spray deposited. Moreover, the PCBM absorption peak at 325 nm is significantly reduced in the *p*-xylene-sprayed film. Reduced PCBM film coverage may explain the absorption loss as PCBM appears to be bound in the crystallites. This is decidedly different than the chlorobenzene-sprayed films where polymer ordering is less pronounced and the PCBM-rich phases are not as well defined.

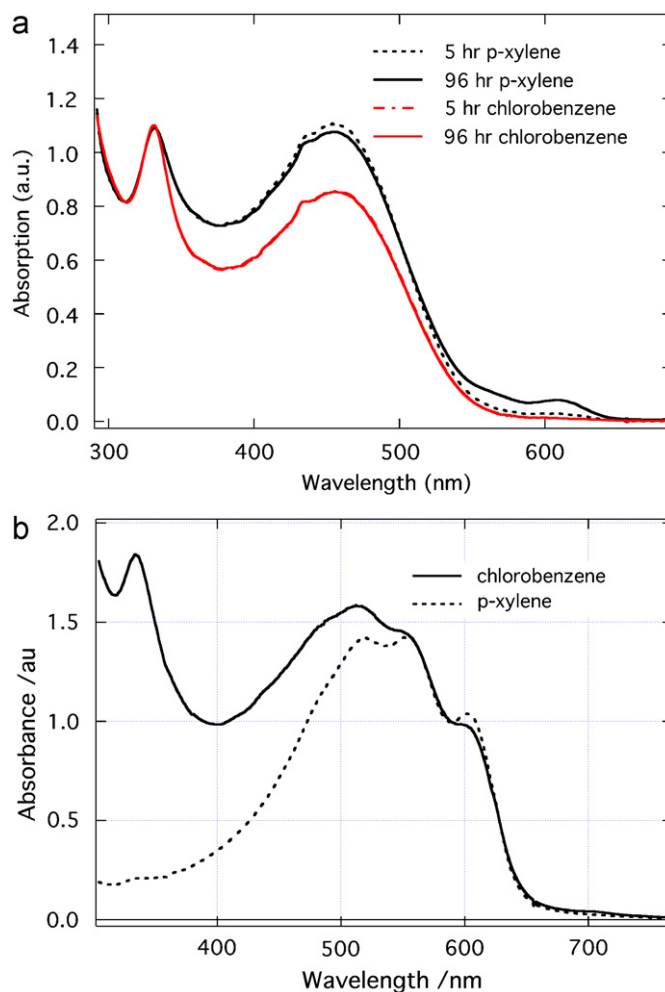
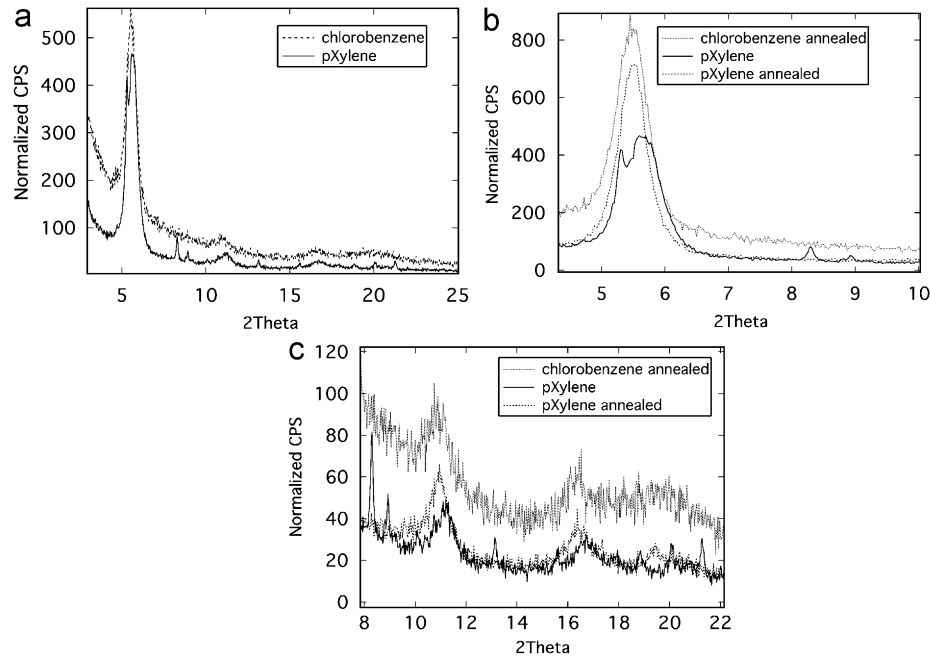


Fig. 3. (a) UV-vis absorption spectra for P3HT:PCBM solutions for time after removal from stirring hotplate and left at room temperature ( $22^\circ\text{C}$ ) normalized at 325 nm. Increased order is shown over time for the *p*-xylene solution. (b) UV-vis absorption of annealed films sprayed from chlorobenzene and *p*-xylene. Films sprayed from *p*-xylene show lower absorption in the blue region resulting from PCBM crystal aggregation. Spectra are shown without normalization.



**Fig. 4.** (a) XRD spectra of sprayed BHJ from *p*-xylene and chlorobenzene normalized for thickness. Films sprayed from the *p*-xylene solution show unique structure. (b) XRD spectra of sprayed BHJ from chlorobenzene, *p*-xylene and annealed *p*-xylene normalized for thickness. A splitting of the P3HT planar separation distance occurs in films sprayed from the *p*-xylene solution and is shown to disappear when annealed. (c) XRD spectra of sprayed BHJ from chlorobenzene, *p*-xylene and annealed *p*-xylene normalized for thickness. Pure PCBM structure is present [24].

To better understand the microscopic structural properties of sprayed films, small-angle XRD spectra were taken and normalized for thickness as described in the experimental section. Spectra are shown for films sprayed from each solvent and for an annealed *p*-xylene-sprayed film in Fig. 4. The chlorobenzene-sprayed film is identical to that of a film prepared by drop casting P3HT:PCBM chlorobenzene solution (not shown). The diffraction patterns of P3HT:PCBM films cast from chlorobenzene have been well documented [24] and here correspond to an interplanar polymer separation of 1.61 nm (*a*-axis) in perfect agreement with literature values. The *p*-xylene-sprayed film, however, shows a splitting in the planar separation distance. Gaussian fits to the double peak in the *p*-xylene-sprayed film spectra correspond to planar separations of 1.67 and 1.57 nm. This differs from the accepted singular interplanar spacing between stacked P3HT backbones [25]. Additionally, Fig. 4b shows further deviation from typical P3HT:PCBM BHJ morphology with the appearance of unique phases, some of which correspond to pristine PCBM film morphology [24]. The individual PCBM peaks and high degree of structure in films sprayed from *p*-xylene are indicators of extreme phase segregation. As evident in Fig. 4 the measured spectrum largely returns to the expected microscopic morphology and 1.61 nm planar separation distance when the *p*-xylene-sprayed film is annealed.

In order to compare these morphological effects observed above on solar cell performance, devices were fabricated with sprayed P3HT:PCBM active layers using chlorobenzene as a solvent with and without a flood layer and from *p*-xylene sprayed at 25 °C as well as at an elevated temperature of 78 °C as described in the experimental section. After fabrication, some devices were subjected to annealing also described in the experimental section. Illuminated current density versus voltage measurements (*JV*) are plotted in Fig. 5. Device performance averaged from six solar cells on each substrate is summarized in Table 2. For our purposes series resistance ( $R_s$ ) and shunt resistance ( $R_{sh}$ ) are defined as the inverse slope at +1 V and -1 V, respectively. Post-fabrication annealing significantly improved

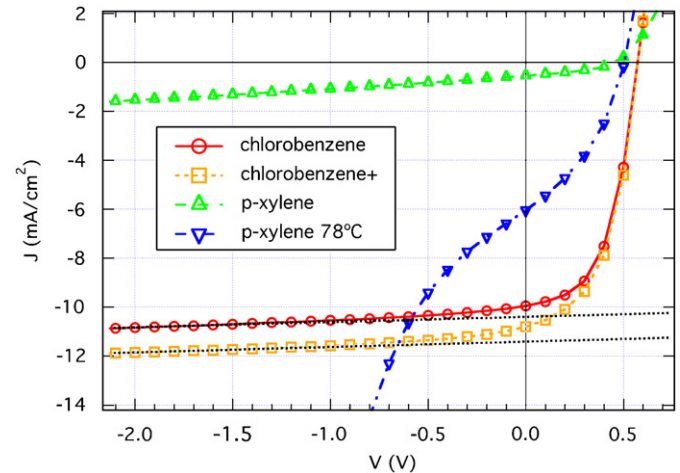


**Fig. 5.** *JV* curves for OPV devices utilizing ultrasonically sprayed BHJ films from chlorobenzene with and without a flood layer, *p*-xylene and *p*-xylene deposited with the substrate held at 78 °C. Lines are fitted to reverse biased currents between -5 and -1 V for chlorobenzene devices.

performance of all devices. Improved phase segregation morphology is evident as the reduction in  $R_s$  and improved short circuit current density ( $J_{sc}$ ) for all devices suggest [16]. The remainder of this article will focus on the post-annealed devices. The *p*-xylene deposited device has good  $V_{oc}$  of 454 mV and FF of 39% but very low  $J_{sc}$  of 0.6 mA/cm<sup>2</sup> and high  $R_s$  of 1268 Ω resulting in a power conversion efficiency of 0.1%. The low  $J_{sc}$  may have resulted from the extensive phase separation observed in Fig 2c, which is confirmed by the loss of absorption from PCBM in the blue part of the absorption spectra and supported by PCBM ordering in the XRD spectra. The high  $R_s$  may have resulted from this extensive BHJ phase segregation or simply poor contact to the crystalline BHJ morphology. The *p*-xylene device deposited at a higher temperature shows improvement relative to the lower

**Table 2**  
Average device properties for solar cells with P3HT:PCBM spray deposited from chlorobenzene without and with a texture-smoothing flood layer or from *p*-xylene deposited at 25 and 78 °C.

BHJ dep.	$V_{oc}$ (mV)	$J_{sc}$ (mA/cm <sup>2</sup> )	Fill factor ( $\times 100$ )	Efficiency (%)	$R_{sh}$ ( $\Omega$ )	$R_s$ ( $\Omega$ )
<i>Device averages—as-deposited</i>						
CB 50	581	8.1	48	2.2	9.3E+06	120
CB 50+	583	8.9	46	2.4	1.2E+07	118
<i>p</i> -Xyl	488	0.3	37	0.05	1.1E+07	1431
<i>p</i> -Xyl 78 °C	269	4.9	32	0.4	1.0E+02	95
<i>Device averages—annealed</i>						
CB 50	582	10.2	51	3.0	6.8E+06	77
CB 50+	576	11.1	51	3.2	8.5E+06	84
<i>p</i> -Xyl	454	0.6	39	0.10	9.8E+06	1268
<i>p</i> -Xyl 78 °C	484	6.0	42	1.2	1.3E+02	63

temperature-deposited crystalline counterpart. An order of magnitude increase in  $J_{sc}$  directly transfers to a PCE of 1.2%. This device also shows improved  $R_s$  but coffee stain effects resulting from the higher temperature deposition likely resulted in the low  $R_{sh}$  minimizing any gains due to improved phase domain morphology. The chlorobenzene-deposited device showed high  $J_{sc}$  of 10.2 mA/cm<sup>2</sup> and FF of 51 resulting in a PCE of 3.0%. The chlorobenzene-deposited device with additional flood layers further improved the PCE to 3.2% mostly due to an increase in  $J_{sc}$ . The smoothing of the active layer electrode interface did not enhance the open-circuit voltage ( $V_{oc}$ ) as might have been expected. Increased device thickness and absorption may not entirely explain the higher  $J_{sc}$  in the chlorobenzene-deposited device with the added flood layers and further investigation of device properties is necessary.

An inspection of the  $JV$  curves reveals much lower current generation for the *p*-xylene-sprayed device over the entire curve than those of the high-temperature-deposited *p*-xylene device and either of the chlorobenzene-deposited devices indicating the possibility of charge separation inefficiency resulting from poor blend morphology [26] or poor interfacial contact to the BHJ layer. Intensity-dependent  $J_{sc}$  data are shown in Fig. 6, and were collected in order to investigate recombination in conjunction with the blend morphology. The fitted lines correspond to the power law dependence of  $J_{sc}$  on intensity.

$$J_{sc}(P_I) = AP_I^\alpha$$

A power of  $\alpha = 1$  indicates no bimolecular recombination as the  $J_{sc}$  is dominated entirely by first-order recombination. A power of  $\alpha = \frac{1}{2}$  corresponds to bimolecular recombination dominating the  $J_{sc}$  characteristics [27]. The powers for the chlorobenzene, chlorobenzene with flood layers, *p*-xylene and high-temperature-deposited *p*-xylene are 0.88, 0.86, 0.67 and 0.85, respectively. The chlorobenzene, the chlorobenzene with flood layers and the high-temperature *p*-xylene-deposited devices exhibit similar power law dependencies within the precision of the experiment. The crystalline *p*-xylene-sprayed device displays the greatest current loss from second-order recombination in this set of devices. Dominant bimolecular recombination and reduced charge separation efficiency in the crystalline *p*-xylene-deposited device is indicative of extended phase segregation in the BHJ film [24].

Measurements of photoinduced current at large reverse bias voltages were performed in order to compare the monomolecular loss component of  $J_{sc}$ . Under one Sun illumination, current was measured for voltage sweeps from  $-10$  to  $+3$  V. Extracting the  $J_{sc}$  intercept at zero bias and calculating the percent of current loss as shown in Fig. 5 is an indicator of the amount of current lost from first-order recombination [28]. Significant current leakage oc-

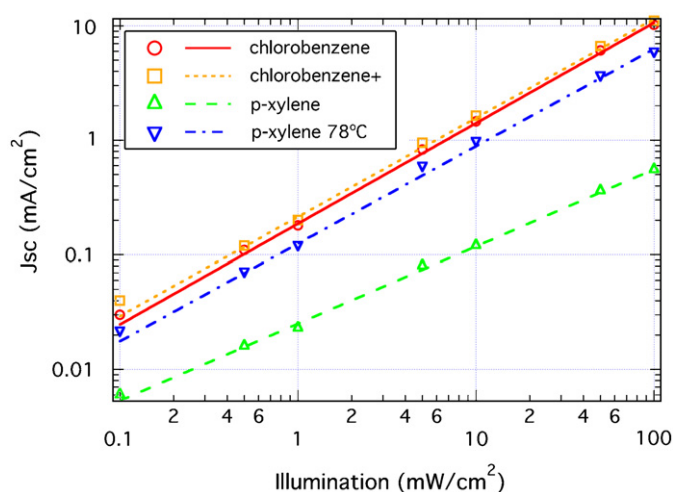


**Fig. 6.**  $J_{sc}$  versus Illumination intensity for OPV devices utilizing ultrasonically sprayed BHJ films from chlorobenzene with and without a flood layer, *p*-xylene and *p*-xylene deposited with the substrate held at 78 °C.

curred for *p*-xylene-deposited devices, preventing a linear fit. Linear regimes were observed for chlorobenzene-deposited devices for reverse bias voltages up to  $-10$  V. The losses due to monomolecular recombination from the chlorobenzene-sprayed devices without and with the flood layer are 4.3% and 5.3%, respectively. Within the precision of the measurement, no recombination mechanistic changes are seen when a flooded layer is added to the chlorobenzene-deposited device. The flood layer has relatively little effect on the bulk device properties although there is significant smoothing of the surface texture. Therefore, the increase in  $J_{sc}$  is likely due to increased absorption.

In this study, ultrasonic spray deposition has yielded devices sprayed from chlorobenzene with power conversion efficiencies of 3.2% further demonstrating commercial viability for OPV manufacturing. We conclude that *p*-xylene, although an interesting solvent for forming crystalline aggregates in P3HT:PCBM sprayed films, currently requires advanced processing methods similar to nanofibrillar purification in order to produce phase segregation and film morphologies that result in high efficiency for photovoltaic applications [14,15]. Solvent blending may incorporate the desired wetting properties of *p*-xylene and preferred phase segregation of chlorobenzene. The main loss mechanisms for the *p*-xylene-sprayed device in this study are extreme phase separation of the active layer components, reduced exciton dissociation due to the lack of intimate mixing, and dominant second-order recombination. Unique phases in the *p*-xylene-sprayed

P3HT:PCBM film were observed and likely contributed to poor device performance. Smoother film surfaces and improved device performance are obtained with chlorobenzene when compared with *p*-xylene as a spray medium.

## Acknowledgments

This work was supported by the US Department of Energy under Contract no. DE-AC36-99GO10337 with the National Renewable Energy Laboratory.

## References

- [1] C.K. Chiang, M.A. Druy, S.C. Gau, A.J. Heeger, E.J. Louis, A.G. MacDiarmid, Y.W. Park, H. Shirakawa, Synthesis of highly conducting films of derivatives of polyacetylene, (CH)<sub>x</sub>, *J. Am. Chem. Soc.* 100 (1978) 1013.
- [2] N.S. Sariciftci, L. Smilowitz, A.J. Heeger, F. Wudl, Photoinduced electron transfer from a conducting polymer to a buckminsterfullerene, *Science* 258 (1992) 1474.
- [3] G. Yu, J. Gao, J.C. Hummelen, F. Wudl, A.J. Heeger, Polymer photovoltaic cells: enhanced efficiencies via a network of internal donor–acceptor heterojunctions, *Science* 270 (1995) 1789.
- [4] J.J.M. Halls, C.A. Walsh, N.C. Greenham, E.A. Marseglia, R.H. Friend, S.C. Moratti, A.B. Holmes, Efficient photodiodes from interpenetrating polymer networks, *Nature* 376 (1995) 498.
- [5] M.A. Green, K. Emery, Y. Hishikawa, W. Warta, Solar cell efficiency tables (version 32), *Prog. Photovoltaics* 16 (2008) 435.
- [6] Personal communication.
- [7] M.O. Reese, A.J. Morpha, M.S. White, N. Kopidakis, S.E. Shaheen, G. Rumbles, D.S. Ginley, Pathways for the degradation of organic photovoltaic P3HT: PCBM based devices, *Sol. Energy Mater. Sol. Cells* 92 (2008) 746.
- [8] M. Jorgensen, K. Norrman, F.C. Krebs, Stability of polymer solar cells, *Sol. Energy Mater. Sol. Cells* 92 (2008) 686.
- [9] C.J. Brabec, J.R. Durrant, Solution-processed organic solar cells, *MRS Bull.* 33 (2008) 670.
- [10] D. Vak, S. Kim, J. Jo, S. Oh, S. Na, J. Kim, D. Kim, Fabrication of organic bulk heterojunction solar cells by a spray deposition method for low-cost power generation, *Appl. Phys. Lett.* 91 (2007) 081102.
- [11] R. Green, A. Morpha, A.J. Ferguson, N. Kopidakis, G. Rumbles, S.E. Shaheen, Performance of bulk heterojunction photovoltaic devices prepared by airbrush spray deposition, *Appl. Phys. Lett.* 92 (2008) 33301.
- [12] M.O. Reese, M.S. White, G. Rumbles, D.S. Ginley, S.E. Shaheen, Optimal negative electrodes for poly(3-hexylthiophene):[6,6]-phenyl C61-butyric acid methyl ester bulk heterojunction photovoltaic devices, *Appl. Phys. Lett.* 92 (2008) 053307.
- [13] G. Li, V. Shrotriya, J. Huang, Y. Yao, T. Moriarty, K. Emery, Y. Yang, High-efficiency solution processable polymer photovoltaic cells by self-organization of polymer blends, *Nat. Mater.* 4 (2005) 864.
- [14] Kyo Jin Ihn, Jeff Moulton, Paul Smith, Whiskers of poly(3-alkylthiophene)s, *J. Polym. Sci. B: Polym. Phys.* 31 (1993) 735.
- [15] S. Berson, R. De Bettignies, S. Bailly, S. Guillerez, Poly(3-hexylthiophene) fibers for photovoltaic applications, *Adv. Funct. Mater.* 17 (2007) 1377.
- [16] W. Ma, C. Yang, X. Gong, K. Lee, A.J. Heeger, Thermally stable, efficient polymer solar cells with nanoscale control of the interpenetrating network morphology, *Adv. Funct. Mater.* 15 (2005) 1617.
- [17] S.E. Shaheen, C.J. Brabec, N.S. Sariciftci, F. Padinger, T. Fromherz, J.C. Hummelen, 2.5% efficient organic plastic solar cells, *Appl. Phys. Lett.* 78 (2001) 841.
- [18] C.N. Hoth, S.A. Choulis, P. Schilinsky, C.J. Brabec, High photovoltaic performance of inkjet printed polymer:fullerene blends, *Adv. Mater.* 19 (2007) 3973.
- [19] R.D. Deegan, O. Bakajin, T.F. Dupont, G. Huber, S.R. Nagel, T.A. Witten, Capillary flow as the cause of ring stains from dried liquid drops, *Nature* 389 (1997) 827.
- [20] T. Ishikawa, M. Nakamura, K. Fujita, T. Tsutsui, Preparation of organic bulk heterojunction photovoltaic cells by evaporative spray deposition from ultradilute solution, *Appl. Phys. Lett.* 84 (2004) 2424.
- [21] M. Campoy-Quiles, Morphology evolution via self-organization and lateral and vertical diffusion in polymer:fullerene solar cell blends, *Nat. Mater.* 7 (2008) 158.
- [22] R. Osterbacka, et al., Two-dimensional electronic excitations in self assembled conjugated polymer nanocrystals, *Science* 287 (2000) 839.
- [23] P. Vanlaeke, G. Vanhoyland, T. Aernouts, D. Cheyns, C. Deibel, J. Manca, P. Heremans, J. Poortmans, Polythiophene based bulk heterojunction solar cells: morphology and its implications, *Thin Solid Films* 511 (2006) 358.
- [24] T. Erb, U. Zhokhavets, G. Gobsch, S. Raleva, B. Stühn, P. Schilinsky, C. Waldauf, C.J. Brabec, Correlation between structural and optical properties of composite polymer/fullerene films for organic solar cells, *Adv. Funct. Mater.* 15 (2005) 1193.
- [25] T. Chen, X. Wu, R.D. Reike, Regiocontrolled synthesis of poly(3-alkylthiophenes) mediated by Rieke zinc: their characterization and solid-state properties, *J. Am. Chem. Soc.* 117 (1995) 233.
- [26] C. Waldauf, M.C. Scharber, P. Schilinsky, J.A. Hauch, C.J. Brabec, Physics of organic bulk heterojunction devices for photovoltaic applications, *J. Appl. Phys.* 99 (2006) 104503.
- [27] I. Riedel, J. Parisi, V. Dyakonov, L. Lutsen, D. Vanderzande, J.C. Hummelen, Effect of temperature and illumination on the electrical characteristics of polymer–fullerene bulk-heterojunction solar cells, *Adv. Funct. Mater.* 14 (2004) 38.
- [28] P. Schilinsky, Ph.D. Thesis, University of Oldenburg, Germany, 2005.